ADVANCED SCIENCE Open Access
www.advancedscience.com

# Electric-Field Control of Low Damping Constant in Epitaxial $Co_2FeSi/LiNbO_3$ Multiferroic Heterostructures

*Shinya Yamada,* Takamasa Usami, Sachio Komori, Yoshio Miura,* Kazuto Yamanoi, Yukio Nozaki, Tomoyasu Taniyama, and Kohei Hamaya**

**To develop electric-field control of magnetization dynamics in a magnetic material for magnonic devices with low-energy power consumption operation, an epitaxial half-metallic $Co_2FeSi/LiNbO_3$ multiferroic heterostructure is experimentally demonstrated. The epitaxial $Co_2FeSi/LiNbO_3$ multiferroic heterostructure shows a low damping constant ($\alpha$) of ∼0.006 and the value of $\alpha$ is decreased to ∼0.004 by applying an electric field. This means that the magnetization dynamics in an epitaxial half-metallic $Co_2FeSi$ layer can be controlled via the piezoelectric strain of $LiNbO_3$ through the magnetoelastic coupling. This study leads to a way toward the realization of magnonic devices with low-energy power consumption operation.**

## 1. Introduction

Magnonics, which utilizes magnetization dynamics and spin wave propagation in a magnetic material as information carriers for processing, offers promising potentialities for novel computing and data processing approaches because of the absence of Joule heating.[1–6] For developing magnonic devices, lots of studies on magnetization dynamics and spin wave propagation in magnetic materials have been reported.[7–10] One of the conventional methods to excite magnetization dynamics and to manipulate spin wave propagation in a magnetic material is to apply an external microwave magnetic field. However, this method has been considered to be energy-inefficient and impractical for device integration.[11] From the viewpoint of low-energy power consumption operation and high device integration, electric-field control of magnetization dynamics and of spin wave propagation is desirable.[12–16]

To achieve this, the use of ferromagnetic/piezoelectric multiferroic heterostructures is one of the potential candidates because the magnetoelectric coupling can control the magnetic properties in the heterostructures above room temperature.[12–20] Until now, electric-field control of magnetization dynamics has been demonstrated in $La_{1-x}Sr_xMnO_3$-/$Pb(Mg_{1/3}Nb_{2/3})O_3$-$PbTiO_3$ (PMN-PT) multiferroic heterostructures.[14,15] However, the value of damping constant ($\alpha$) for the $La_{1-x}Sr_xMnO_3$ film was ∼0.01,[14,15] insufficient for magnonic and spin-wave device applications.

For long-distance spin wave transport, the use of a magnetic material with a low $\alpha$ is essential. In addition, it is important to use a high-quality epitaxial film because spin wave transport properties correlate with the crystallinity and the crystal orientation in the magnetic film.[8,10] Among a variety of magnetic materials, Co-based Heusler alloys with the chemical formula $Co_2YZ$, where $Y$ is a transition metal and $Z$ is a main group element,

S. Yamada, T. Usami, Y. Miura, K. Hamaya
Center for Spintronics Research Network
Graduate School of Engineering Science
The University of Osaka
1-3 Machikaneyama, Toyonaka, Osaka 560-8531, Japan
E-mail: yamada.shinya.es@osaka-u.ac.jp; miura@kit.ac.jp; hamaya.kohei.es@osaka-u.ac.jp

S. Yamada, T. Usami, K. Hamaya
Spintronics Research Network Division
Institute for Open and Transdisciplinary Research Initiatives
The University of Osaka
2-1 Yamadaoka, Suita, Osaka 565-0871, Japan

The ORCID identification number(s) for the author(s) of this article can be found under https://doi.org/10.1002/advs.202511250



**DOI: 10.1002/advs.202511250**

S. Komori, T. Taniyama
Department of Physics
Nagoya University
Chikusa-ku, Nagoya, Aichi 464-8602, Japan

Y. Miura
Faculty of Electrical Engineering and Electronics
Kyoto Institute of Technology
Matsugasaki, Sakyo-ku, Kyoto 606-8585, Japan

Y. Miura
Research Center for Magnetic and Spintronic Materials
National Institute for Materials Science (NIMS)
Tsukuba, Ibaraki 305-0047, Japan

K. Yamanoi, Y. Nozaki
Department of Physics
Keio University
Yokohama, Kanagawa 223-8522, Japan

K. Yamanoi, Y. Nozaki
Center for Spintronics Research Network
Keio University
Yokohama, Kanagawa 223-8522, Japan

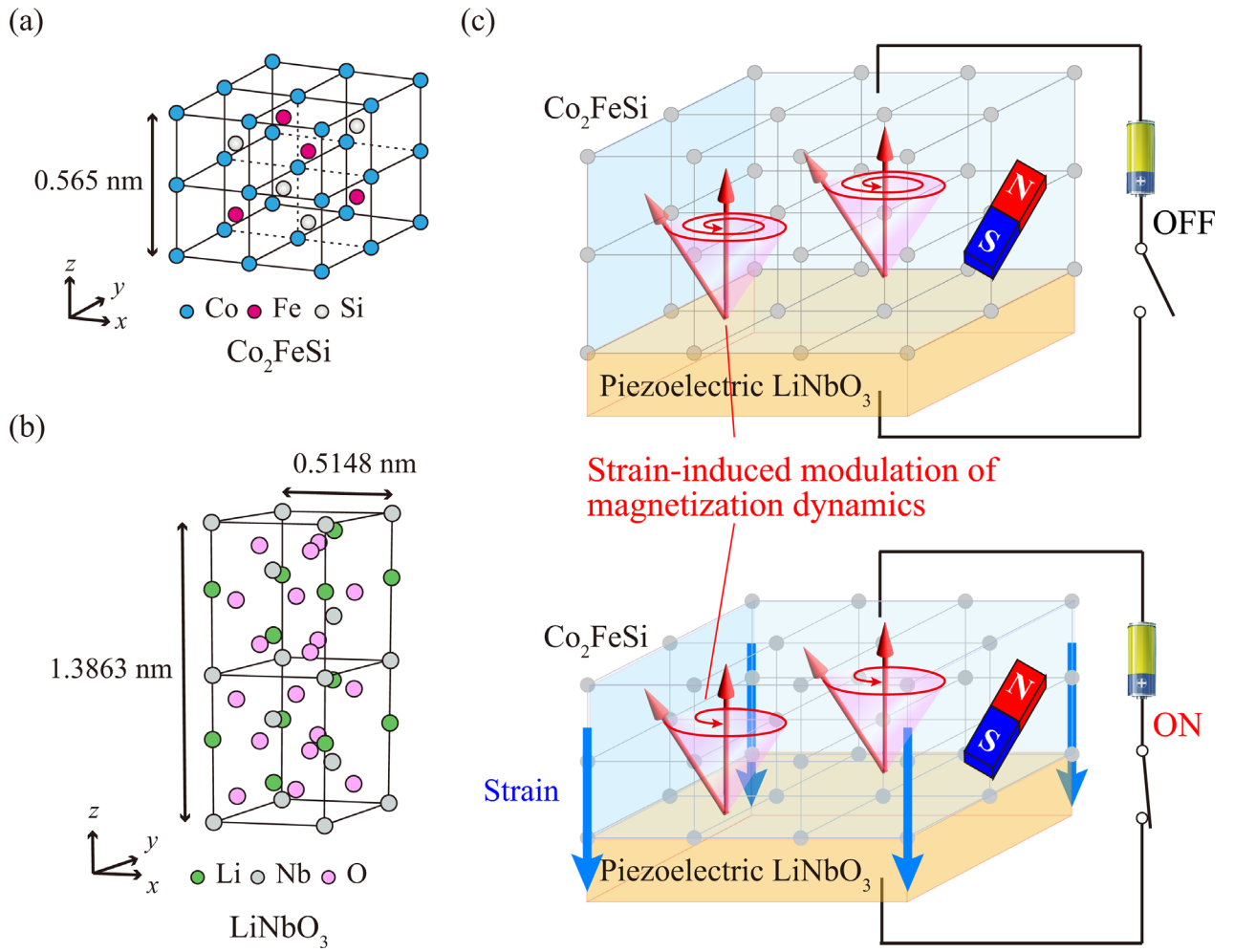


**Figure 1.** Crystal structures of a) $L2_1$-ordered $Co_2FeSi$ and b) $LiNbO_3$. c) Schematic representation of the concept of this study. The lattice strain induced by piezoelectric $LiNbO_3$ modulates the magnetization dynamics in $Co_2FeSi$ through the magnetoelastic coupling.

are considered as candidate materials because many of them possess high spin polarization, low $\alpha$, high Curie temperature, and so on.[21–28] In particular, $Co_2FeSi$, one of the half-metallic Co-based Heusler alloys,[29] has shown not only high room-temperature spin polarization[30,31] and low $\alpha$ values (0.0023 – 0.0061)[32] in single-crystalline epitaxial films but also intriguing effects such as a giant converse magnetoelectric effect[16,18–20,33,34] and electric-field control of anisotropic magnetoresistance[35] in $Co_2FeSi$/piezoelectric interfacial multiferroic systems.

Until now, $Co_2YZ$/piezoelectric multiferroic heterostructures such as $Co_2YZ/BaTiO_3$[34,35] and $Co_2YZ$/PMN-PT[16,18–20,33,36–39] have been intensively studied. However, piezoelectric $LiNbO_3$, where surface acoustic waves (SAW) have been utilized to excite spin wave resonance in a magnetic material,[40] has not thus far been explored as a growth substrate because the crystal structure of $L2_1$-ordered $Co_2YZ$ (cubic structure) is completely different from $LiNbO_3$ (trigonal ilmenite structure) and there is no matching between the lattice length and the symmetry, as shown in **Figure** 1a,b.

In this research article, we demonstrate an epitaxial half-metallic $Co_2FeSi/LiNbO_3$ multiferroic heterostructures with a low $\alpha$. It is noted that the value of $\alpha$ in the epitaxial $Co_2FeSi$ layer is decreased from ~0.006 to ~0.004 by applying an electric field. This means that the magnetization dynamics in the epitaxial $Co_2FeSi$ layer can be controlled via the piezoelectric lattice strain of $LiNbO_3$ through the magnetoelastic coupling. We discuss the possible origin of the strain-induced modulation of $\alpha$ in $Co_2FeSi$ from the first-principles calculation.

## 2. Results and Discussion

### 2.1. Epitaxial $Co_2FeSi/LiNbO_3$ Heterostructures

The concept of this study is schematically represented in Figure 1c. The lattice strain induced by the piezoelectric $LiNbO_3$ modulates the magnetization dynamics in $Co_2FeSi$ through the magnetoelastic coupling. For the growth of an epitaxial $Co_2FeSi$ layer, $LiNbO_3$ 128° Y-cut (LN-128Y) substrates were used.[41] To solve the atomic arrangement mismatch problem between $Co_2FeSi$ and LN-128Y (Figure 1a,b), we propose the use of Chromium (Cr) with a bcc crystal structure as an insertion layer.[41] Cr has been widely used as a buffer layer for the growth

of epitaxial Heusler-alloy films on oxide substrates.[26,42–44] Although the crystal structure and the atomic arrangement between bcc-Cr and $LiNbO_3$ are also completely different, it was reported that molybdenum (Mo) with a bcc crystal structure was epitaxially grown on LN-128Y.[45,46] Therefore, Cr can be used as an insertion layer for the growth of an epitaxial $Co_2FeSi$ layer on LN-128Y.

Epitaxial $Co_2FeSi$ films were grown on LN-128Y substrates by molecular beam epitaxy (MBE). The details of the growth process are described in the Experimental section (Supporting Information). Representative reflection high-energy electron diffraction (RHEED) images during the growth are shown in Figure S1a–c (Supporting Information). After the LN-128Y substrates were annealed at 500 °C for one hour in an MBE chamber, a 10-nm-thick Cr insertion layer is grown at a substrate temperature of 200 °C. As we conceived, clear streak patterns due to good 2D epitaxial growth are observed, as shown in Figure S1b (Supporting Information). Subsequently, a 30-nm-thick $Co_2FeSi$ layer is grown at a substrate temperature of 200 °C by co-evaporating Co, Fe, and Si using Knudsen cells.[47–49] After the growth of $Co_2FeSi$, streak patterns due to epitaxial growth are observed, as shown in Figure S1a (Supporting Information). To confirm the effect of an insertion of the Cr layer, we also use Vanadium (V) with a bcc crystal structure as an insertion layer.[50] As a result, although the surface flatness of a V insertion layer is not good compared with that of the Cr one (Figure S1e, Supporting Information), epitaxial growth of $Co_2FeSi$ is realized, as shown in Figure S1d (Supporting Information). By the way, if we directly grew $Co_2FeSi$ on LN-128Y, only polycrystalline films could be obtained as shown in Figure S1f (Supporting Information). These results mean that the insertion of a bcc metal layer is essential to demonstrate epitaxial $Co_2FeSi$/LN-128Y heterostructures.

To investigate the crystal orientation of the epitaxial $Co_2FeSi$/LN-128Y heterostructures, we performed x-ray diffraction (XRD) measurements. **Figure 2a** shows the pole figure of the $Co_2FeSi(220)$ plane for the epitaxial $Co_2FeSi$/LN-128Y heterostructure. Star and circle symbols represent the diffraction peaks of LN(0001) and $Co_2FeSi(220)$, respectively, and the LN(0001) peak is superimposed on the $Co_2FeSi(220)$ peaks ($\phi = 0°$, $\chi = 38°$). From this figure, it is revealed that the epitaxial $Co_2FeSi$ layer forms two crystal domains in the film plane, as shown in the circles of Figure 2a, and the $Co_2FeSi(110)$ plane is tilted at an angle of 38° from out-of-plane direction, as shown in a blue arrow of Figure 2b. This unique epitaxial relationship is the same as in the reported previous studies of epitaxial bcc-Mo/LN-128Y heterostructures.[45,46] As shown in the red arrows, although the mismatch between $Co_2FeSi$ (~0.849 nm) and $LiNbO_3$ (~0.892 nm) is ~5 %, the Cr insertion layer decreases the mismatch between $Co_2FeSi$ and $LiNbO_3$. As a result, epitaxial growth of $Co_2FeSi$ on LN-128Y is realized through the Cr insertion layer, as illustrated in Figure 2b.

To examine the effect of an electric field ($E$) on the lattice strain in the $Co_2FeSi$ layer, we also performed XRD measurements by applying $E$. Figure 2c,d shows the XRD $2\theta$-$\omega$ scan measurements of the $Co_2FeSi(111)$ and (220) planes for the epitaxial $Co_2FeSi$ layer at $E = -10$ kV/cm (blue), 0 (black), and +10 kV/cm (red). To roughly confirm whether piezoelectric distortion propagated by external electric fields, electric fields were applied at only three points: −10 kV/cm, 0, and +10 kV/cm. From Figure 2a,b, there are no Miller indices corresponding to the vertical and horizontal directions of the epitaxial $Co_2FeSi$ layer, therefore, we assumed that the [111] and [$1\bar{1}0$] directions of $Co_2FeSi$ are the vertical and horizontal directions of the epitaxial $Co_2FeSi$ layer, as illustrated in Figure 2e. In Figure 2c, the $Co_2FeSi(111)$ peak due to the formation of the $L2_1$-ordered structure can be seen. By sweeping $E$ from −10 to +10 kV/cm, diffraction peaks of the $Co_2FeSi(111)$ plane move toward higher angles. This indicates that the compressive (tensile) strain is applied along the out-of-plane direction by applying a positive (negative) $E$. For the (220) plane, on the other hand, we can see no peak shift before and after applying $E$. That is, while the in-plane lattice constant ($a'$) does not change with respect to $E$, the out-of-plane lattice strain constant ($c'$) is varied by applying $E$ and positive (negative) $E$ induces the out-of-plane compressive (tensile) strain in the epitaxial $Co_2FeSi$ layer. This feature can be qualitatively understood from the piezoelectric lattice strain of $LiNbO_3$.

We further carried out structural characterizations by cross-sectional high-angle annular dark-field scanning transmission electron microscopy (HAADF-STEM) and energy dispersive x-ray spectroscopy (EDX) measurements. Figure 2f–k shows a HAADF-STEM image and EDX mapping ones for each element of an epitaxial $Co_2FeSi$/LN-128Y heterostructure. A Cr layer with a flat surface is grown on an LN-128Y substrate (Figure 2f). Because of the low-temperature growth of 200 °C, atomic interdiffusion between the Cr insertion layer and the LN-128Y substrate is suppressed (Figure 2g,h). On top of the flat Cr layer, a $Co_2FeSi$ layer is grown with suppressed atomic interdiffusion (Figure 2h-k). These results indicate that our low-temperature MBE techniques enable us to demonstrate an epitaxial $Co_2FeSi$/LN-128Y heterostructure without degrading piezoelectric properties of $LiNbO_3$.

We also measured magnetic properties of the epitaxial $Co_2FeSi$/LN-128Y heterostructure. A field-dependent magnetization ($M$-$H$ curve) at 300 K for an epitaxial $Co_2FeSi$/LN-128Y heterostructure in a high magnetic field region is shown in Figure S2a (Supporting Information), where an external magnetic field was applied was applied with an angle of 90° with respect to the LN[$2\bar{1}\bar{1}0$] direction (a red arrow in the inset figure). The saturation magnetization is ~1235 emu/cc, almost equivalent to that for bulk[29] and thin-film[47,48,51] samples reported previously. In-plane normalized $M$-$H$ curves in a low magnetic field region are also shown in Figure S2b (Supporting Information). The epitaxial $Co_2FeSi$/LN-128Y heterostructure exhibits a strong in-plane uniaxial magnetic anisotropy with an easy axis of the perpendicular to the LN[$2\bar{1}\bar{1}0$] direction. We speculate that the in-plane uniaxial magnetic anisotropy is derived from the lattice strain induced by the change in the crystal structure from the substrate.[52–56] From these structural characterizations and magnetic properties, we regard that epitaxial $Co_2FeSi$/LN-128Y multiferroic heterostructures are successfully grown by MBE techniques.

### 2.2. Magnetization Dynamics

We measured the magnetization dynamics of $Co_2FeSi$/LN-128Y multiferroic heterostructures. The experimental set up for ferromagnetic resonance (FMR) measurements is shown in **Figure 3a**. The details of the measurements are described in the Experimen-

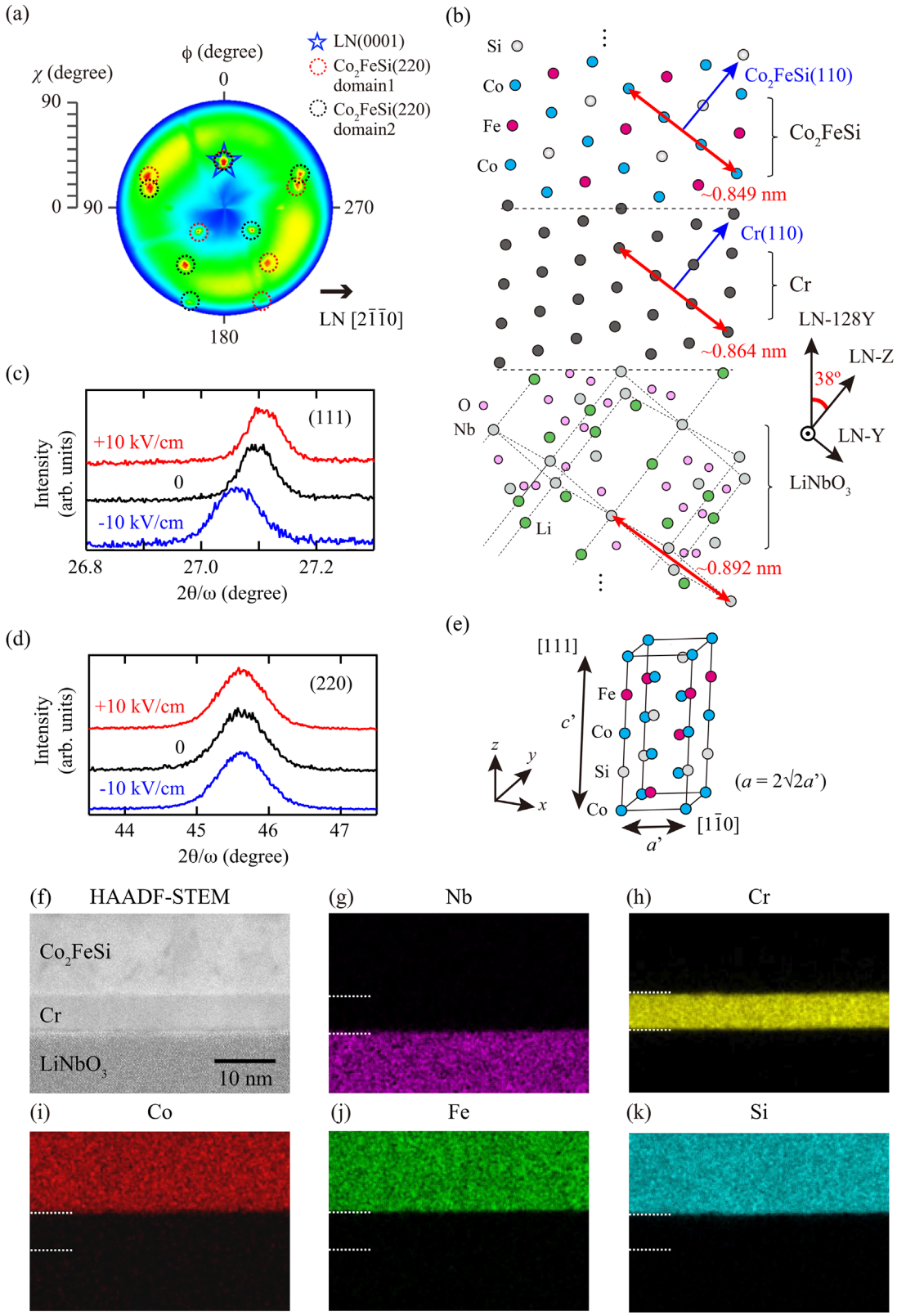


**Figure 2.** a) XRD pole figure of the $Co_2FeSi$(220) plane for an epitaxial $Co_2FeSi$/LN-128Y heterostructure. b) Schematic of the cross-sectional view of the epitaxial $Co_2FeSi$/LN-128Y multiferroic heterostructure. c,d) XRD 2$\theta$-$\omega$ scan measurements of the $Co_2FeSi$(111) and $Co_2FeSi$(220) planes for an epitaxial $Co_2FeSi$/LN-128Y multiferroic heterostructure under applying $E$. Schematic of the XRD 2$\theta$-$\omega$ scan measurements is shown in (e). f–k) HAADF-STEM image and EDX mapping images for each element in an epitaxial $Co_2FeSi$/LN-128Y heterostructure.

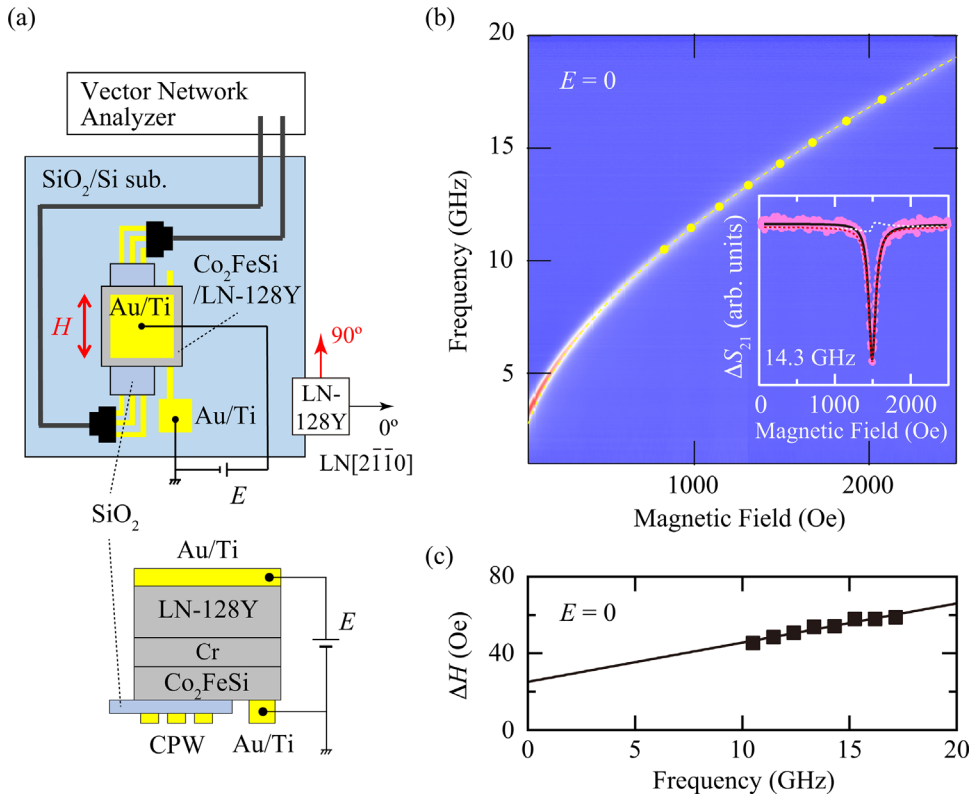


**Figure 3.** a) Top view of the experimental setup for FMR measurements. b) FMR spectra map for an epitaxial $Co_2FeSi$/LN-128Y multiferroic heterostructure at $E = 0$, where the external static magnetic fields were applied along the magnetic easy axis of the $Co_2FeSi$ layer (at an angle of 90° with respect to the LN[2$\bar{1}\bar{1}$0] direction, red arrow in the figure). A representative FMR spectrum is shown in the inset. c) Frequency dependence of $\Delta H$ at $E = 0$.

tal Section (Supporting Information). Figure 3b shows the FMR spectra map for the epitaxial $Co_2FeSi$/LN-128Y multiferroic heterostructure at $E = 0$, where the external static magnetic fields were applied along the magnetic easy axis of the epitaxial $Co_2FeSi$ layer (a red arrow in Figure 3a). A representative FMR spectrum is shown in the inset. A clear FMR absorption with a small linewidth is observed. The FMR spectra are fitted with the following equation, which consists of symmetric and antisymmetric Lorentzians,[57]

$$\Delta S_{21} = C_s \frac{(\Delta H)^2}{(\Delta H)^2 + (H - H_{res})^2} + C_{as} \frac{\Delta H(H - H_{res})}{(\Delta H)^2 + (H - H_{res})^2} + B, \quad (1)$$

where $C_s$ and $C_{as}$ are the parameters representing the amplitude of the symmetric and antisymmetric Lorentzians, $B$ is the parameter representing the offset, $\Delta H$ is the half-width at half maximum, and $H_{res}$ is the resonant field. A fitting curve is shown as the solid black curve in the inset of Figure 3(b). Here since spin wave excitation with a wavelength near the line width of the coplaner waveguide (CPW) antenna is not necessary to be considered, the dispersion relationship between the resonant frequency ($f_{res}$) and $H_{res}$ is fitted using Kittel's equation,[58,59]

$$f_{res} = \left(\frac{1}{2\pi}\right)\left(\frac{ge}{2m_0 c}\right)\sqrt{(H_{res} + H_a)(H_{res} + H_a + 4\pi M_{eff})}, \quad (2)$$

where, $g$ is the $g$ factor (= 2),[60] $e$ is the electron charge, $m_0$ is the electron rest mass, $c$ is the velocity of light, $H_a$ is the anisotropic field, and $M_{eff}$ is the effective magnetization. Figure 3c shows the extracted values of $\Delta H$ versus $f_{res}$ for the epitaxial $Co_2FeSi$/LN-128Y multiferroic heterostructure. A clear linear relation between $\Delta H$ and $f_{res}$ can be seen. From the frequency dependence of $\Delta H$ and the following equation,[61,62]

$$\Delta H = \Delta H_0 + \frac{2\pi\alpha f_{res}}{\gamma}, \quad (3)$$

where $\gamma$ is the gyromagnetic ratio and $\Delta H_0$ is the inhomogeneous broadening, the value of $\alpha$ is estimated to be ~0.006, comparable to those for highly-ordered epitaxial Co-based Heusler-alloy films.[32,63–67] Although the $\alpha$ value of ~0.006 is small, the influence of the presence of two crystal domains in the epitaxial $Co_2FeSi$ layer on $\alpha$ needs to be considered because the epitaxial $Co_2FeSi$ layer is an imperfect single-crystalline film. These results show that epitaxial half-metallic $Co_2FeSi$/LN-128Y multiferroic heterostructures with a low $\alpha$ are obtained.

### 2.3. Effect of Strain on Damping Constant

We investigated the effect of $E$ on the magnetization dynamics of an epitaxial $Co_2FeSi$/LN-128Y multiferroic heterostructure. Using the experimental setup shown in Figure 3a, we performed FMR measurements under applying $E$. For each measurement, we analyzed the data by following the same procedure as described above. **Figure 4** shows $\alpha$ versus $E$ for the epi-

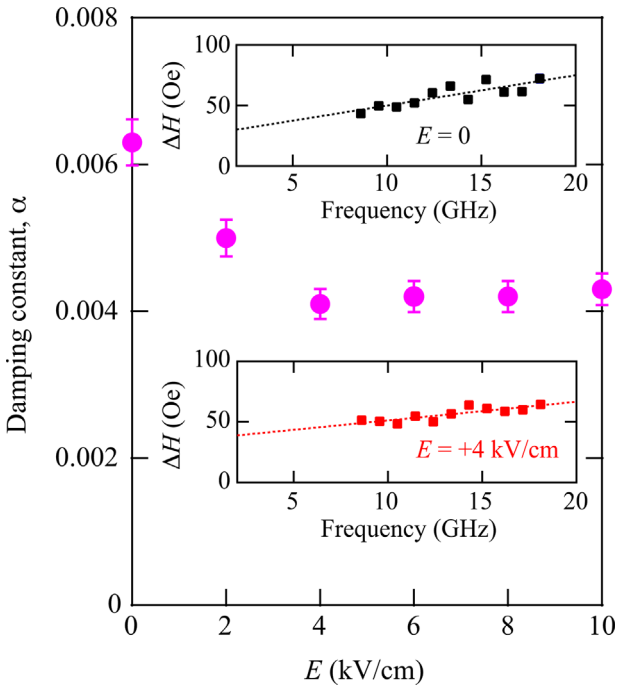


**Figure 4.** $\alpha$ versus $E$ for an epitaxial $Co_2FeSi$/LN-128Y multiferroic heterostructure. The inset graphs show frequency dependence of $\Delta H$ at $E$ = 0 (upper, black) and +4 kV/cm (lower, red).

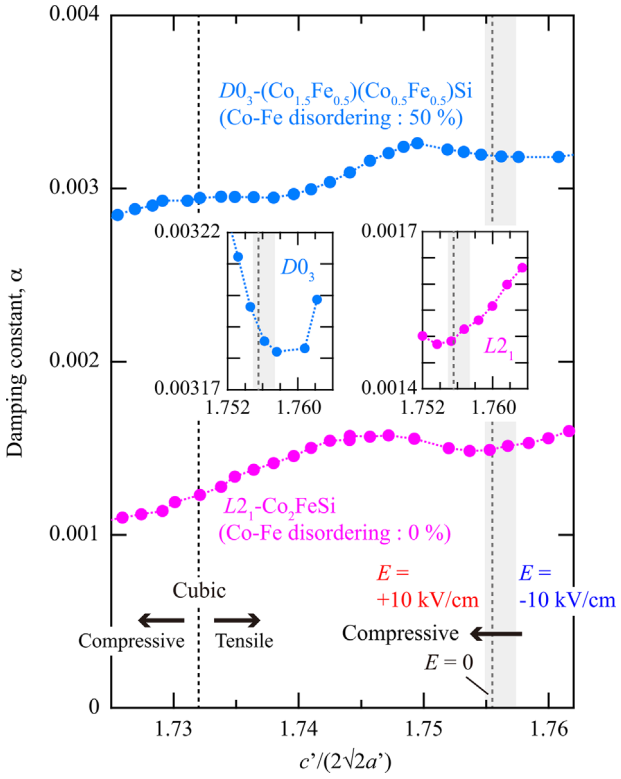


**Figure 5.** Theoretical values of $\alpha$ versus lattice strain, $c'/(2\sqrt{2}a')$, for $Co_2FeSi$ with the Co–Fe disordering of 0 % ($L2_1$-$Co_2FeSi$, magenta plots) and 50 % ($D0_3$-$(Co_{1.5}Fe_{0.5})(Co_{0.5}Fe_{0.5})Si$, cyan plots). Gray area is the experimental region of $c'/(2\sqrt{2}a')$ calculated from the results in Figure 2c,d. The inset graphs show the enlarged views near $c'/(2\sqrt{2}a')$ of 1.756 for $L2_1$-$Co_2FeSi$ (right, magenta plots) and $D0_3$-$(Co_{1.5}Fe_{0.5})(Co_{0.5}Fe_{0.5})Si$ (left, cyan plots).

taxial $Co_2FeSi$/LN-128Y multiferroic heterostructure. The inset graphs show the representative $f$ dependence of $\Delta H$. The value of $\alpha$ is decreased from ~0.006 to ~0.004 by applying positive $E$. This means that the magnetization dynamics in the epitaxial $Co_2FeSi$ layer can be modulated by applying $E$. We also notice an increase in $\Delta H_0$ applying $E$ (inset figures), which is probably due to the magnetic inhomogeneity in the ferromagnetic domains induced by the lattice distortion from the piezoelectric LN-128Y substrates. Although the electric-field modulation of $\alpha$ was reported in $La_{1-x}Sr_xMnO_3$/PMN-PT multiferroic heterostructures, the modulation of $\alpha$ was in the order of ~$10^{-2}$.[14,15] For the epitaxial $Co_2FeSi$/LN-128Y multiferroic heterostructure, on the other hand, the magnitude of $\alpha$ is modulated in the order of $10^{-3}$. The Curie temperature of $Co_2FeSi$ is 1100 K,[29] much higher than that of $La_{1-x}Sr_xMnO_3$ (~370 K),[68,69] and $Co_2FeSi$ has exhibited specific features in multiferroic heterostructures.[16,18–20,33–35] Therefore, it is expected that the epitaxial $Co_2FeSi$/LN-128Y multiferroic heterostructures with a low $\alpha$ present a potential of the application for electric-field-controllable magnonic devices.

To understand the effect of the lattice strain on $\alpha$, we performed the first-principles calculations of $\alpha$ for $Co_2FeSi$ versus the lattice strain. The details of the first-principles calculations are described in the Experimental Section (Supporting Information). As mentioned in the Section 2.1, there are no Miller indices corresponding to the vertical and horizontal directions of the epitaxial $Co_2FeSi$ layer, we assume that the out-of-plane of the $Co_2FeSi$ layer is defined as the $Co_2FeSi$[111] direction, as shown in Figure 2e. Since $D0_3$-type disordering can easily occur in $Co_2FeSi$ even for the low-temperature growth,[51] we also considered the effect of structural disordering on $\alpha$. **Figure 5** displays the theoretical results of $\alpha$ versus lattice strain, $c'/(2\sqrt{2}a')$, for $Co_2FeSi$ without the Co–Fe disordering ($L2_1$-$Co_2FeSi$, magenta) and with the 50% Co–Fe disordering ($D0_3$-$(Co_{1.5}Fe_{0.5})(Co_{0.5}Fe_{0.5})Si$, cyan). The dotted magenta line at $c'/(2\sqrt{2}a')$ of 1.732 is the case of cubic-$Co_2FeSi$. There is a large discrepancy in the magnitude of $\alpha$ between experiment and theory since the theoretical calculations do not include imperfection of the crystal and magnetic structures. As shown in Figure 2a, the epitaxial $Co_2FeSi$ layer contains two crystal domains in the film plane, which can become one of the possible reasons of the discrepancy in $\alpha$ between experiment and theory. The presence of some structural disorder and lattice strain in the epitaxial $Co_2FeSi$ layer also affects the discrepancy in $\alpha$. Although the Cr insertion layer is antiferromagnetic, exchange bias cannot be observed from the low-field $M$-$H$ curves in Figure S2b (Supporting Information). In addition, when the thickness of the $Co_2FeSi$ layer was decreased from 30 to 10 nm without changing the thickness of the Cr layer, the value of $\alpha$ was also ~0.006 and exchange bias could not be observed from low-field $M$-$H$ curves (not shown here). From these, we can judge that the influence of the exchange coupling between $Co_2FeSi$ and Cr is negligible and the mechanism of the modulation of $\alpha$ observed here is derived predominantly from the strain effect. Therefore, we compare the

qualitative behavior of $\alpha$ with respect to $c'/(2\sqrt{2}a')$ between experiment and theory.

The theoretical value of $\alpha$ for cubic $D0_3$-$(Co_{1.5}Fe_{0.5})(Co_{0.5}Fe_{0.5})Si$ is larger than cubic $L2_1$-$Co_2FeSi$ because of the increase in the total DOS in the minority spin band at the Fermi level ($E_F$), as shown in Figure S3a–d (Supporting Information). According to the theoretical model proposed by Kambersky[70] and Gilmore *et al.*,[71] it is predicted that the spin-flip scattering can be strongly suppressed in half-metallic materials because only a majority spin band exists at $E_F$.[72] As the total DOS in the minority spin band at $E_F$ decreases, the spin-flip scattering is suppressed, leading to a decrease in $\alpha$. The theoretical $\alpha$ values near $c'/(2\sqrt{2}a')$ of 1.732 (cubic-$Co_2FeSi$) tend to be small when the compressive strain is applied for both $L2_1$-$Co_2FeSi$ and $D0_3$-$(Co_{1.5}Fe_{0.5})(Co_{0.5}Fe_{0.5})Si$. This indicates that theoretical studies also suggest the value of $\alpha$ in the epitaxial $Co_2FeSi$ layer can be controlled by the lattice strain in piezoelectric $LiNbO_3$ through the magnetoelastic coupling. From the XRD data in Figure 2c,d, the value of $c'/(2\sqrt{2}a')$ was estimated to be ~1.756 at $E = 0$ (a gray dotted line in Figure 5), indicating that the out-of-plane tensile strain is applied before applying $E$, probably caused by the crystal structural difference between $Co_2FeSi$ (and Cr) and $LiNbO_3$. Focusing on the data near $c'/(2\sqrt{2}a')$ of 1.756 (a gray area in Figure 5), the theoretical values of $\alpha$ for $L2_1$-$Co_2FeSi$ tend to decrease by applying the compressive strain (right inset figure) while those for $D0_3$-$(Co_{1.5}Fe_{0.5})(Co_{0.5}Fe_{0.5})Si$ increase (left inset figure), therefore our experimental data are qualitatively consistent with the behavior of $L2_1$-$Co_2FeSi$. Thus, we roughly judged that our epitaxial $Co_2FeSi$ layer contains relatively little $D0_3$-type disorder. Considering the fact that the values of the in-plane lattice constant do not change by $E$ (Figure 2d), we speculate that the application of the out-of-plane compressive strain to the epitaxial $Co_2FeSi$ layer induces the structural change toward the cubic-$Co_2FeSi$, leading to the decrease in $\alpha$. At present, since only a qualitative interpretation of the phenomenon observed here is presented, further consideration will be needed to understand the modulation mechanism in $Co_2FeSi/LiNbO_3$ multiferroic systems in details.

Finally, we comment on the superiority of this study. Contrary to $Co_2FeSi$/PMN-PT[16,18–20,33] and $Co_2FeSi/BaTiO_3$[34,35] multiferroic heterostructures, the epitaxial $Co_2FeSi/LiNbO_3$ multiferroic heterostructures are not influenced by ferroelectric domain structures in the piezoelectric $LiNbO_3$ substrate because $LiNbO_3$ has a uniform single ferroelectric domain structure. This is one of the important points in terms of controllability of magnetization dynamics. In addition, if spin wave generation by SAW on piezoelectric $LiNbO_3$ substrates[40,73,74] was implemented in our epitaxial $Co_2FeSi/LiNbO_3$ multiferroic heterostructures, electric-field generation of spin waves could be demonstrated in the $Co_2FeSi$/LN-128Y multiferroic heterostructures. Furthermore, if antiferromagnetic materials were utilized in this multiferroic heterostructure, magnetization dynamics of antiferromagnetic materials could also be modulated via the strain-induced variation of the density of states near the Fermi level.[75–77] Therefore, we expect that the epitaxial half-metallic $Co_2FeSi$/LN-128Y multiferroic heterostructures developed here lead to a step toward the realization of electric-field-operatable magnonic devices.

## 3. Conclusion

We have demonstrated epitaxial half-metallic $Co_2FeSi/LiNbO_3$ multiferroic heterostructures by introducing a bcc-Cr insertion layer. The epitaxial $L2_1$-$Co_2FeSi/LiNbO_3$ heterostructures showed a high saturation magnetization almost equivalent to theoretical values reported previously and a low damping constant of ~0.006, indicating a half-metallic nature. The values of $\alpha$ were modulated from ~0.006 to ~0.004 by applying an electric field, qualitatively explained in terms of the strain-induced variation of the density of states near the Fermi level. This study leads to a step toward the realization of electric-field-operatable magnonic devices.

## Supporting Information

Supporting Information is available from the Wiley Online Library or from the author.

## Acknowledgements

The authors would like to thank Prof. Y. Suzuki and Mr. S. Nagata of The University of Osaka for lots of experimental supports. This work was supported by JST CREST Grant Nos. JPMJCR18J1, JPMJCR19J4, JST Super Highway Grant No. J231130012, JSPS KAKENHI Grant Nos. JP23KK0086, JP24H00034, JP24H00380, JP24K17309, JP24K23033, JP25K01266, JST FOREST Grant No. JPMJFR212V, the Kazuchika Okura Memorial Foundation, and the Spintronics Research Network of Japan (Spin-RNJ).

## Conflict of Interest

The authors declare no conflict of interest.

## Data Availability Statement

The data that support the findings of this study are available from the corresponding author upon reasonable request.

## Keywords

Heusler alloys, $LiNbO_3$, magnetization dynamics, multiferroic heterostructures

Received: June 18, 2025
Revised: July 22, 2025
Published online:

[1] S. Neusser, D. Grundler, *Adv. Mater.* **2009**, *21*, 2927.
[2] A. Khitun, M. Bao, K. L. Wang, *J. Phys. D: Appl. Phys.* **2010**, *43*, 264005.
[3] V. V. Kruglyak, S. O. Demokritov, D. Grundler, *J. Phys. D: Appl. Phys.* **2010**, *43*, 264001.
[4] A. V. Chumak, A. A. Serga, B. Hillebrands, *Nat. Commun.* **2014**, *5*, 4700.
[5] A. V. Chumak, V. I. Vasyuchka, A. A. Serga, B. Hillebrands, *Nat. Phys.* **2015**, *11*, 453.
[6] A. V. Chumak, A. A. Serga, B. Hillebrands, *J. Phys. D: Appl. Phys.* **2017**, *50*, 244001.

[7] M. Bailleul, D. Olligs, C. Fermon, S. O. Demokritov, *Europhys. Lett.* **2001**, *56*, 741.
[8] R. Yilgin, Y. Sakuraba, M. Oogane, S. Mizukami, Y. Ando, T. Miyazaki, *Jpn. J. Appl. Phys.* **2007**, *46*, L205.
[9] K. Yamanoi, S. Yakata, T. Kimura, T. Manago, *Jpn. J. Appl. Phys.* **2013**, *52*, 083001.
[10] K. Sekiguchi, S.-W. Lee, H. Sukegawa, N. Sato, S.-H. Oh, R. D McMichael, K.-J. Lee, *NPG Asia Mater.* **2017**, *9*, e392.
[11] S. Husain, I. Harris, P. Meisenheimer, S. Mantri, X. Li, M. Ramesh, P. Behera, H. Taghinejad, J. Kim, P. Kavle, S. Zhou, T. Y. Kim, H. Zhang, P. Stevenson, J. G. Analytis, D. Schlom, S. Salahuddin, J. Íñiguez-González, B. Xu, L. W. Martin, L. Caretta, Y. Han, L. Bellaiche, Z. Yao, R. Ramesh, *Nat. Commun.* **2024**, *15*, 5966.
[12] H. Qin, R. Dreyer, G. Woltersdorf, T. Taniyama, S. van Dijken, *Adv. Mater.* **2021**, *33*, 2100646.
[13] W. Zhu, H. Qin, L. Flajsman, T. Taniyama, S. van Dijken, *Appl. Phys. Lett.* **2022**, *120*, 112407.
[14] A. Das, Mrinalini, T. Usami, S. P. Pati, T. Taniyama, V. Gorige, *J. Phys.: Condens. Matter.* **2023**, *35*, 285801.
[15] A. Das, Mrinalini, T. Usami, S. P. Pati, S. Komori, T. Taniyama, V. Gorige, *J. Alloys Compd.* **2024**, *1009*, 176866.
[16] T. Taniyama, Y. Gohda, K. Hamaya, T. Kimura, *Sci. Technol. Adv. Mater.* **2024**, *25*, 2412970.
[17] T. Taniyama, *J. Phys.: Condens. Matter.* **2015**, *27*, 504001.
[18] S. Fujii, T. Usami, Y. Shiratsuchi, A. M. Kerrigan, A. M. Yatmeidhy, S. Yamada, T. Kanashima, R. Nakatani, V. K. Lazarov, T. Oguchi, Y. Gohda, K. Hamaya, *NPG Asia Mater.* **2022**, *14*, 43.
[19] J. Okabayashi, T. Usami, A. M. Yatmeidhy, Y. Murakami, Y. Shiratsuchi, R. Nakatani, Y. Gohda, K. Hamaya, *NPG Asia Mater.* **2024**, *16*, 3.
[20] T. Usami, Y. Sanada, S. Fujii, S. Yamada, Y. Shiratsuchi, R. Nakatani, K. Hamaya, *Adv. Sci.* **2024**, *12*, 2413566.
[21] I. Galanakis, P. H. Dederichs, N. Papanikolaou, *Phys. Rev. B* **2002**, *66*, 174429.
[22] Y. Sakuraba, M. Hattori, M. Oogane, Y. Ando, H. Kato, A. Sakuma, T. Miyazaki, H. Kubota, *Appl. Phys. Lett.* **2006**, *88*, 192508.
[23] K. Inomata, N. Ikeda, N. Tezuka, R. Goto, S. Sugimoto, M. Wojcik, E. Jedryka, *Sci. Technol. Adv. Mater.* **2008**, *9*, 014101.
[24] R. Shan, H. Sukegawa, W. H. Wang, M. Kodzuka, T. Furubayashi, T. Ohkubo, S. Mitani, K. Inomata, K. Hono, *Phys. Rev. Lett.* **2009**, *102*, 246601.
[25] A. Boehnke, U. Martens, C. Sterwerf, A. Niesen, T. Huebner, M. von der Ehe, M. Meinert, T. Kuschel, A. Thomas, C. Heiliger, M. Münzenberg, G. Reiss, *Nat. Commun.* **2017**, *8*, 1626.
[26] K. Elphick, W. Frost, M. Samiepour, T. Kubota, K. Takanashi, H. Sukegawa, S. Mitani, A. Hirohata, *Sci. Technol. Adv. Mater.* **2021**, *22*, 235.
[27] Z. Zhang, E. Liu, X. Lu, W. Zhang, Y. You, G. Xu, Z. Xu, P. K. J. Wong, Y. Wang, B. Liu, X. Yu, J. Wu, Y. Xu, A. T. S. Wee, F. Xu, *Adv. Funct. Mater.* **2021**, *31*, 2007211.
[28] M. Wang, C. Pan, N. Xie, X. Qiu, Y. Li, L. Lang, S. Wang, D. Cheng, W. Fan, S.-M. Zhou, Z. Shi, *Adv. Sci.* **2025**, *12*, 2407171.
[29] S. Wurmehl, G. H. Fecher, H. C. Kandpal, V. Ksenofontov, C. Felser, H.-Ji Lin, J. Morais, *Phys. Rev. B* **2005**, *72*, 184434.
[30] T. Kimura, N. Hashimoto, S. Yamada, M. Miyao, K. Hamaya, *NPG Asia Mater.* **2012**, *4*, e9.
[31] K. Hamaya, N. Hashimoto, S. Oki, S. Yamada, M. Miyao, T. Kimura, *Phys. Rev. B* **2012**, *85*, 100404(R).
[32] Y. Kasatani, S. Yamada, H. Itoh, M. Miyao, K. Hamaya, Y. Nozaki, *Appl. Phys. Express* **2014**, *7*, 123001.
[33] T. Usami, S. Fujii, S. Yamada, Y. Shiratsuchi, R. Nakatani, K. Hamaya, *Appl. Phys. Lett.* **2022**, *118*, 142402.
[34] S. Hu, S. Yamada, P.-C. Chang, W.-C. Lin, K. Hamaya, T. Kimura, *Phys. Rev. Applied* **2023**, *20*, 034029.
[35] S. Yamada, Y. Teramoto, D. Matsumi, D. Kepaptsoglou, I. Azaceta, T. Murata, K. Kudo, V. K. Lazarov, T. Taniyama, K. Hamaya, *Phys. Rev. Mater.* **2021**, *5*, 014412.
[36] C. Zhou, F. Wang, G. Dunzhu, J. Yao, C. Jiang, *J. Phys. D: Appl. Phys.* **2016**, *49*, 455001.
[37] C. Zhou, G. Dunzhu, J. Yao, C. Jian, *J. Alloys Compd.* **2017**, *710*, 680.
[38] G. Dunzhu, F. Wang, C. Zhou, C. Jiang, *Nanoscale Res. Lett.* **2018**, *13*, 75.
[39] G. Dunzhu, F. Liu, Y. Wang, C. Zhou, C. Jiang, *Mater. Res. Express* **2019**, *6*, 066114.
[40] M. Weiler, L. Dreher, C. Heeg, H. Huebl, R. Gross, M. S. Brandt, S. T. B. Goennenwein, *Phys. Rev. Lett.* **2011**, *106*, 117601.
[41] S. Yamada, T. Usami, S. Komori, S. Nagata, Y. Nozaki, T. Taniyama, K. Hamaya, "Epitaxial $Co_2FeSi/LiNbO_3$ multiferroic heterostructures with a low damping constant,"*2023 IEEE International Magnetic Conference - Short Papers (INTERMAG Short Papers)* **2023**, *1–2*. https://doi.org/10.1109/INTERMAGShortPapers58606.2023.10228793
[42] Y. Sakuraba, J. Nakata, M. Oogane, H. Kubota, Y. Ando, A. Sakuma, T. Miyazaki, *Jpn. J. Appl. Phys.* **2005**, *44*, 6535.
[43] N. Tezuka, N. Ikeda, S. Sugimoto, K. Inomata, *Jpn. J. Appl. Phys.* **2007**, *46*, L454.
[44] K. Inomata, N. Ikeda, N. Tezuka, R. Goto, S. Sugimoto, M. Wojcik, E. Jedryka, *Sci. Technol. Adv. Mater.* **2008**, *9*, 014101.
[45] V. Polewczyk, M. Hehn, A. Hillion, S. Robert, P. Boulet, K. Dumesnil, *J. Phys.: Condens. Matter.* **2019**, *31*, 405801.
[46] V. Polewczyk, M. Hehn, A. Hillion, S. Robert, P. Boulet, K. Dumesnil, *J. Phys.: Condens. Matter.* **2020**, *32*, 235803.
[47] S. Yamada, K. Hamaya, K. Yamamoto, T. Murakami, K. Mibu, M. Miyao, *Appl. Phys. Lett.* **2010**, *96*, 082511.
[48] S. Yamada, K. Tanikawa, S. Oki, M. Kawano, M. Miyao, K. Hamaya, *Appl. Phys. Lett.* **2014**, *105*, 071601.
[49] Y. Fujita, M. Yamada, M. Tsukahara, T. Oka, S. Yamada, T. Kanashima, K. Sawano, K. Hamaya, *Phys. Rev. Applied* **2017**, *8*, 014007.
[50] C. Guillemard, S. Petit-Watelot, T. Devolder, L. Pasquier, P. Boulet, S. Migot, J. Ghanbaja, F. Bertran, S. Andrieu, *J. Appl. Phys.* **2020**, *128*, 241102.
[51] K. Kudo, Y. Hamazaki, S. Yamada, S. Abo, Y. Gohda, K. Hamaya, *ACS Appl. Electron. Mater.* **2019**, *1*, 2371.
[52] A. Yamaguchi, T. Ohkochi, A. Yasui, T. Kinoshita, K. Yamada, *IEEE Trans. Magn.* **2017**, *53*, 8108504.
[53] A. Yamaguchi, A. Nakao, T. Ohkochi, A. Yasui, T. Kinoshita, Y. Utsumi, T. Saiki, K. Yamada, *AIP Adv.* **2018**, *8*, 056411.
[54] R. Nakamura, S. Saegusa, S. Suzuki, A. Nakao, Y. Utsumi, T. Ohkochi, M. Oura, Y. Takizawa, T. Saiki, T. Lee, K. J. Kim, K. Yamada, T. Ogasawara, A. Yamaguchi, *Sensor Mater.* **2019**, *31*, 3007.
[55] M. Ito, A. Yamaguchi, D. Oshima, T. Kato, M. Shima, K. Yamada, *Appl. Phys. Lett.* **2021**, *119*, 152407.
[56] M. Ito, S. Ono, H. Fukui, K. Kogirima, N. Maki, T. Hikage, T. Kato, T. Ohkochi, A. Yamaguchi, M. Shima, K. Yamada, *J. Magn. Magn. Mater.* **2022**, *564*, 170177.
[57] N. Mecking, Y. S. Gui, C.-M. Hu, *Phys. Rev. B* **2007**, *76*, 224430.
[58] Z. Lai, Z. Li, X. Liu, L. Bai, Y. Tian, W. Mi, *J. Phys. D.: Appl. Phys.* **2018**, *51*, 245001.
[59] V. Thiruvengadam, B. B. Singh, T. Kojima, K. Takanashi, M. Mizuguchi, S. Bedanta, *Appl. Phys. Lett.* **2019**, *115*, 202402.
[60] E. Mancini, F. Pressacco, M. Haertinger, E. E. Fullerton, T. Suzuki, G. Woltersdorf, C. H. Back, *J. Phys. D.: Appl. Phys.* **2013**, *46*, 245302.
[61] T. Usami, M. Itoh, T. Taniyama, *AIP Advances* **2021**, *11*, 045302.
[62] Y. Zhao, Q. Song, S.-H. Yang, T. Su, W. Yuan, S. S. P. Parkin, J. Shi, W. Han, *Sci. Rep.* **2016**, *6*, 22890.
[63] S. Mizukami, D. Watanabe, M. Oogane, Y. Ando, Y. Miura, M. Shirai, T. Miyazaki, *J. Appl. Phys.* **2009**, *105*, 07D306.
[64] M. Oogane, T. Kubota, Y. Kota, S. Mizukami, H. Naganuma, A. Sakuma, Y. Ando, *Appl. Phys. Lett.* **2010**, *96*, 252501.

[65] T. Sebastian, Y. Ohdaira, T. Kubota, P. Pirro, T. Brächer, K. Vogt, A. A. Serga, H. Naganuma, M. Oogane, Y. Ando, B. Hillebrands, *Appl. Phys. Lett.* **2012**, *100*, 112402.
[66] S. Oki, Y. Sasaki, Y. Kasatani, S. Yamada, S. Mizukami, Y. Nozaki, K. Hamaya, *J. Phys.: Condens. Matter.* **2018**, *30*, 255802.
[67] C. J. Love, B. Kuerbanjiang, A. Kerrigan, S. Yamada, K. Hamaya, G. Van Der Laan, V. K. Lazarov, S. A. Cavill, *Appl. Phys. Lett.* **2021**, *119*, 172404.
[68] A. Urushibara, Y. Moritomo, T. Arima, A. Asamitsu, G. Kido, Y. Tokura, *Phys. Rev. B* **1995**, *51*, 14103.
[69] J.-H. Park, E. Vescovo, H.-J. Kim, C. Kwon, R. Ramesh, T. Venkatesan, *Nature* **1998**, *392*, 794.
[70] V. Kamberský, *Phys. Rev. B* **2007**, *76*, 134416.
[71] K. Gilmore, Y. U. Idzerda, M. D. Stiles, *Phys. Rev. Lett.* **2007**, *99*, 027204.
[72] C. Liu, C. K. A. Mewes, M. Chshiev, T. Mewes, W. H. Butler, *Appl. Phys. Lett.* **2009**, *95*, 022509.
[73] Y. Kurimune, M. Matsuo, S. Maekawa, Y. Nozaki, *Phys. Rev. B* **2020**, *102*, 174413.
[74] M. Xu, K. Yamamoto, J. Puebla, K. Baumgaertl, B. Rana, K. Miura, H. Takahashi, D. Grundler, S. Maekawa, Y. Otani, *Sci. Adv.* **2020**, *6*, eabb1724.
[75] Z. Q. Liu, H. Chen, J. M. Wang, J. H. Liu, K. Wang, Z. X. Feng, H. Yan, X. R. Wang, C. B. Jiang, J. M. D. Coey, A. H. MacDonald, *Nat. Electron.* **2019**, *1*, 172.
[76] H. Yan, Z. Feng, S. Shang, X. Wang, Z. Hu, J. Wang, Z. Zhu, H. Wang, Z. Chen, H. Hua, W. Lu, J. Wang, P. Qin, H. Guo, X. Zhou, Z. Leng, Z. Liu, C. Jiang, M. Coey, Z. Liu, *Nat. Nanotechnol.* **2019**, *14*, 131.
[77] Z. Liu, Z. Feng, H. Yan, X. Wang, X. Zhou, P. Qin, H. Guo, R. Yu, C. Jiang, *Adv. Electron. Mater.* **2019**, *5*, 1900176.